Title
Combined in silico/in vivo analysis of mechanisms providing for root apical meristem self-organization and maintenance.

Journal
Annals of botany, 110(2)

ISSN
0305-7364

Authors
Mironova, VV
Omelyanchuk, NA
Novoselova, ES
et al.

Publication Date
2012-07-01

DOI
10.1093/aob/mcs069

Peer reviewed

Annals of Botany **110**: 349–360, 2012
doi:10.1093/aob/mcs069, available online at www.aob.oxfordjournals.org

ANNALS OF BOTANY
Founded 1887

PART OF A SPECIAL ISSUE ON ROOT BIOLOGY

Combined *in silico/in vivo* analysis of mechanisms providing for root apical meristem self-organization and maintenance

V. V. Mironova[1,*], N. A. Omelyanchuk[1], E. S. Novoselova[1], A. V. Doroshkov[1], F. V. Kazantsev[1], A. V. Kochetov[1,2], N. A. Kolchanov[1,2], E. Mjolsness[3,4] and V. A. Likhoshvai[1,2]

[1]*Institute of Cytology and Genetics, SB RAS, Lavrentyeva 10, Novosibirsk, Russia,* [2]*Novosibirsk State University, Pirogova 2, Novosibirsk, Russia,* [3]*Departments of Computer Science and Mathematics, University of California, Irvine, CA, USA and* [4]*Institute for Genomics and Bioinformatics, University of California, Irvine, CA, USA*
* *For correspondence. E-mail kviki@bionet.nsc.ru*

Received: 1 December 2011 Returned for revision: 4 January 2012 Accepted: 14 February 2012 Published electronically: 16 April 2012

• *Background and Aims* The root apical meristem (RAM) is the plant stem cell niche which provides for the formation and continuous development of the root. Auxin is the main regulator of RAM functioning, and auxin maxima coincide with the sites of RAM initiation and maintenance. Auxin gradients are formed due to local auxin biosynthesis and polar auxin transport. The PIN family of auxin transporters plays a critical role in polar auxin transport, and two mechanisms of auxin maximum formation in the RAM based on PIN-mediated auxin transport have been proposed to date: the reverse fountain and the reflected flow mechanisms.
• *Methods* The two mechanisms are combined here in *in silico* studies of auxin distribution in intact roots and roots cut into two pieces in the proximal meristem region. In parallel, corresponding experiments were performed *in vivo* using DR5::GFP *Arabidopsis* plants.
• *Key Results* The reverse fountain and the reflected flow mechanism naturally cooperate for RAM patterning and maintenance in intact root. Regeneration of the RAM in decapitated roots is provided by the reflected flow mechanism. In the excised root tips local auxin biosynthesis either alone or in cooperation with the reverse fountain enables RAM maintenance.
• *Conclusions* The efficiency of a dual-mechanism model in guiding biological experiments on RAM regeneration and maintenance is demonstrated. The model also allows estimation of the concentrations of auxin and PINs in root cells during development and under various treatments. The dual-mechanism model proposed here can be a powerful tool for the study of several different aspects of auxin function in root.

Key words: Auxin response, root apical meristem, patterning, reverse fountain, reflected flow, mathematical model, *Arabidopsis thaliana*.

INTRODUCTION

In higher plants post-embryonic growth is maintained by the activities of meristems, which comprise stem cells and their derivatives, serving as the source of all differentiated cell types. The root apical meristem (RAM) is established at the earliest stages of embryogenesis and is localized to the root apex after germination (Dolan *et al.*, 1993). Accumulating evidence suggests that the plant hormone auxin has the primary role in RAM establishment and patterning (reviewed by Jiang and Feldman, 2005). The distribution of auxin in the root apex as inferred from the activity of auxin-responsive promoter elements DR5 and DII has a concentration maximum in the RAM, namely in the quiescent centre (QC) and root cap initials, with a decreased level in the root cap (Sabatini *et al.*, 1999; Brunoud *et al.*, 2012). The existence of an auxin maximum in the QC was also shown by combining fluorescence-activated cell sorting and highly sensitive mass spectrometry methods (Petersson *et al.*, 2009). This maximum of auxin concentration forms at the earliest stages of RAM initiation, persists at the root tip in development and is restored from provascular cells after RAM structure damage (before RAM regeneration) (Sabatini *et al.*, 1999; Xu *et al.*, 2006).

Auxin gradients have been shown to be formed due to local auxin biosynthesis and/or directional cell-to-cell polar auxin transport (Sabatini *et al.*, 1999; Benkova *et al.*, 2003; Friml *et al.*, 2002; Stepanova *et al.*, 2008; Ikeda *et al.*, 2009; Petersson *et al.*, 2009; Kim *et al.*, 2011). Auxin transport is driven by the asymmetric distribution of different auxin membrane carriers, including AUX/LAX protein family members, p-glycoprotein ABC transporters and PIN family efflux carriers (Bennett *et al.*, 1996; Friml *et al.*, 2003; Blilou *et al.*, 2005; Geisler and Murphy, 2006). PIN family efflux transporters were shown to have a rate-limiting role in auxin efflux and direct auxin flow in plants (Petrásek *et al.*, 2006; Wisniewska *et al.*, 2006). Compared with ABC transporters, the action of PINs is auxin-specific and more sensitive to polar auxin transport inhibitors (Petrásek *et al.*, 2006). *Pin* mutants resemble phenotypes of the wild-type plants treated by auxin transport inhibitors in more aspects than do mutants of ABC transporters (reviewed by Tanaka *et al.*, 2006). In *Arabidopsis*, the PIN-FORMED (PIN) proteins are encoded by functionally

redundant genes so the defects in *pin* mutants are masked by ectopic activity of the remaining *PIN* genes (Blilou *et al.*, 2005; Vieten *et al.*, 2005). In root development, phenotypic defects were revealed only for triple *pin1 pin3 pin4* mutants having very short root and for quadruple *pin1 pin3 pin4 pin7* mutants, which, depending on the ecotype, either are embryo lethal with pronounced root pole abnormalities or develop into seedlings with no root or a non-functional root (Friml *et al.*, 2003). On the other hand, loss of ABC or AUX/LAX transporters does not appear to strongly impact early developmental processes (reviewed by Ugartechea-Chirino *et al.*, 2010; Zažímalová *et al.*, 2010). This provided additional evidence for a critical contribution of PIN proteins to the auxin distribution pattern in the root. In particular, the PIN1, PIN3, PIN4 and PIN7 proteins provide for a continuous acropetal (rootward) auxin flow via the vascular system to the QC cells (Friml *et al.*, 2002; Blilou *et al.*, 2005). PIN3 and PIN7 are also involved in the lateral redistribution of auxin in the root cap. PIN2 proteins mediate basipetal (shootward) auxin transport from the root tip via the epidermis as well as rootward auxin transport in root cortex. Here we use the rootward/shootward directional nomenclature defined by Baskin *et al.* (2010).

The assumption that PIN family efflux carriers are the main contributors to the formation of the auxin distribution pattern in the root was central to two different hypotheses regarding the mechanism responsible for auxin distribution within the root: a 'reverse fountain' (Swarup and Benett, 2003; Grieneisen *et al.*, 2007) and a 'reflected flow' (Likhoshvai *et al.*, 2007; Mironova *et al.*, 2010). According to the concept of the reverse fountain, the rootward and oppositely directed shootward auxin flows are coordinated by lateral auxin redistribution processes to generate and maintain an auxin distribution in the root tip. This mechanism, whereby tissue patterning predetermines the morphogen distribution, could be characterized as a 'structural mechanism' due to the pre-existing structure of PIN-localized expression levels. The 'reflected flow' hypothesis could be referred to a 'positional information' mechanism, where, by contrast, the morphogen distribution determines tissue patterning and anatomical structure (Mironova *et al.*, 2010; Wolpert, 2011). The latter mechanism is based on the auxin-dependent regulation of auxin flow: low auxin concentrations activate the transcription of *PIN1* genes, whereas high concentrations induce degradation of PIN1 proteins. The two mechanisms were tested in two-dimensional (2-D) mathematical models which describe auxin redistribution by diffusion and active transport in a cell layout located at a longitudinal cut of root.

We suggest that the reverse fountain and the reflected flow mechanisms are complementary in root development. In particular, only the reflected flow mechanism operates at the very early stages of root development. At later developmental stages, an anatomical structure forms and provides for the functioning of the reverse fountain mechanism, which allows for more robust maintenance of the auxin maximum in the RAM. However, the reflected flow mechanism does not disappear, revealing itself if RAM structure is disrupted. To test this hypothesis on the complementarity of the two mechanisms, we combined them in a dual-mechanism 2-D mathematical model. In numerical experiments it was shown that the reverse fountain and the reflected flow mechanisms could naturally cooperate due to auxin-regulated expression of auxin transporters. We also investigated the distribution of auxin response in DR5-GFP seedlings with decapitated roots and root tips excised from these seedlings. In decapitated roots the reverse fountain is destroyed and *in silico* experiments showed that the reflected flow mechanism alone may provide for RAM restoration after the root tip is cut off. However, experimentally all excised roots, including the smallest roots with the least tissue left above the QC, were able to maintain the positioning of the auxin maximum for more than 4 d. This could not be explained by the functioning of either the reverse fountain or the reflected flow mechanism, alone or in combination. We tested the role of auxin synthesis in maintenance of an auxin maximum. In these numerical experiments we showed that ubiquitous auxin production at a small but non-zero rate provides for an auxin distribution pattern that agrees with the experimentally recorded auxin response dynamics in the excised root tips. Thus, both computer simulations and experimental validation indicate that auxin biosynthesis is a third force of equal importance to the reverse fountain and reflected flow mechanisms for auxin patterning in the RAM.

MATERIAL AND METHODS

Plant material and root excisions

DR5::GFP seeds were kindly provided by Alexis Peaucelle (INRA Centre de Versailles-Grignon, Versailles, France). *Arabidopsis* seedlings were grown under a 16 : 8-h light–dark cycle at 18 °C on vertically oriented Petri dishes with half-strength MS agar medium containing 1 % sucrose.

The root cut experiments were performed as shown in Fig. 3 below. The root tips of seedlings at 3 d after germination (dag) were dissected manually by a steel blade under a stereomicroscope. An incision was made to the proximal meristem, the exact position varying from plant to plant. Over the next 4 d (6, 24, 48, 72 and 96 h) after dissection changes in green fluorescent protein (GFP) expression were fixed in both the decapitated root and the excised root tip using an LSM 510 META laser scanning microscope or a Zeiss AxioImager M1. Images were processed using ImageJ and AxioVision software. RAM regeneration was confirmed by tip morphology and its gravitropic response.

2-D dual-mechanism mathematical model

Model assumptions. In the present model we consider processes occurring in the RAM. To simplify the model, only three auxin transporters are considered: PIN1, PIN2, and PIN3. PIN1 protein mediates acropetal (rootward) auxin flow in the central cylinder cells; PIN2 is expressed in the epidermis and regulates basipetal (shootward) and lateral inward transport; and PIN3 regulates lateral outward auxin redistribution in the root tip where auxin accumulates. We ignore the redundant mechanisms for PIN2 and PIN3 to mediate rootward auxin flow and for PIN1 to mediate lateral inward auxin transport.

Discussion of PIN protein polarization mechanisms are beyond the scope of the present work. It is assumed that all the PIN protein synthesized in a cell is localized to the cell wall. The localization of PIN proteins is different for the two cell types. PIN1 is located only at the basal (rootward) side

of the central cylinder cell, PIN2 proteins at the apical (shootward) and lateral (inward) cell sides of the epidermis, and PIN3 is expressed and localized ubiquitously (Fig. 1B).

The concentration of PIN proteins in a cell depends on auxin concentration in a cell and is described according to the experimental data of Vieten *et al.* (2005). Auxin activates PIN1–4 and PIN7 transcription at relatively low concentration, whereas at high concentrations, auxin mediates increased degradation of PIN1, PIN2 and PIN7 proteins. Data regarding the effective concentrations of auxin for PIN1, PIN2 and PIN3 regulation from Vieten *et al.* (2005) (Fig. 1C, D) were used for model parameter estimation (see below).

The DR5 reporter was demonstrated to reflect free auxin concentrations between 10^{-8} and 10^{-4} M (Ulmasov *et al.*, 1997; Sabatini *et al.*, 1999). In the model analysis we assume that the auxin concentration in a cell correlates linearly with the auxin response observed by DR5::GFP. This allows us to compare *in vivo* and *in silico* results.

Model description. In the model the dynamics of auxin concentration [*a*] distribution and expression of its transporters [*PIN1*], [*PIN2*] and [*PIN3*] in the root meristem are described based on the interactions of a limited set of intracellular processes, as follows.

Subsystem 1: auxin flow to the root meristem

The rate of auxin flow (V_a) into the meristem from the root elongation zone (shoot-derived or rootward auxin flow) is described by:

$$V_a = \alpha \tag{1}$$

where α is the intensity of auxin flow.

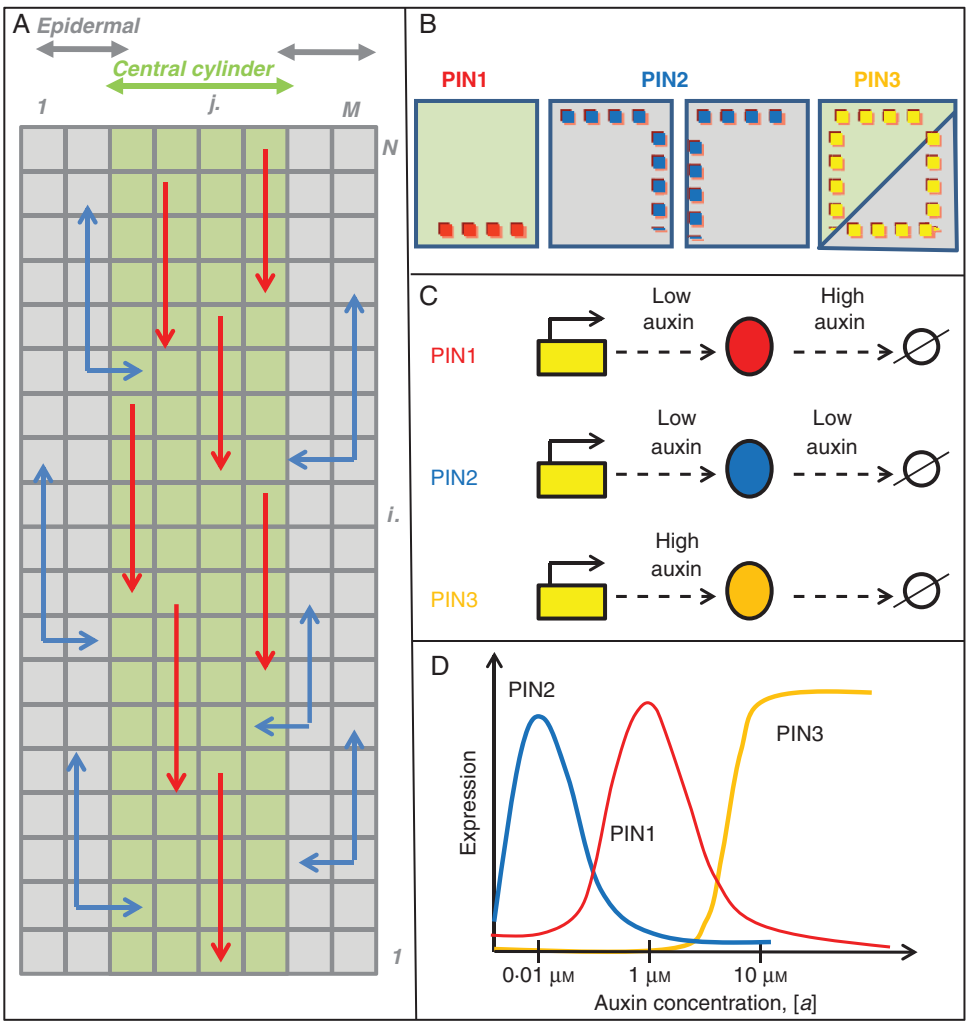

FIG. 1. Schematic representation of the main model assumptions. (A) The cellular layout of the 2-D dual-mechanism model, which represents a longitudinal cut of the root meristem. Only two cell types were specified in the $M \times N$ rectangular layout: epidermal tissue (grey; $j = 1,2$ and $j = M-1, M$) and central cylinder (green; $j = 3, \ldots, M-2$). Layer $i = 1$ is located at the root end; $i = N$ is at the border of the meristematic zone. The auxin transport routes by PIN1 and PIN2 proteins are presented by red and blue arrows, respectively. For simplicity, PIN3, which is considered to transport auxin without specific direction, is not shown. (B) PIN localization within the cells of different types. PIN1 is located basally in a central cylinder cell; PIN2 has basal–lateral expression in the 'epidermal' tissue; and PIN3 may be ubiquitously expressed along the cell membranes of both tissues. (C) The mechanisms of auxin-regulated PIN expression considered in the model according with the data from Vieten *et al.* (2005). (D) Qualitative plot of PIN protein expression versus auxin concentrations based on the mechanisms (C) and experimental data (Vieten *et al.*, 2005).

Subsystem 2: auxin biosynthesis

We examined two variants of auxin synthesis (with the rate $V_{s,a}$) in a root: no synthesis (2a) or auxin is synthesized in a cell at a low rate (2b).

$$V_{s,a} = 0 \quad (2a)$$
$$V_{s,a} = K_{s,a} \quad (2b)$$

where $K_{s,a}$ is the constant of auxin synthesis.

Subsystem 3: auxin degradation

The rate of irreversible loss (degradation) of auxin, $V_{d,a}$, through its utilization or migration from the modelled region is defined as

$$V_{d,a} = K_{d,a} \cdot [a] \quad (3)$$

where $K_{d,a}$ is the rate constant for auxin degradation and $[a]$ is the concentration of auxin.

Subsystem 4: auxin diffusion

We ignore auxin diffusion within the apoplast; instead, auxin is modelled as moving directly from a cell to its neighbours by means of passive diffusion and active transport. The rate of auxin diffusion from one cell to another is described as:

$$V_{diff,a} = D \cdot [a] \quad (4)$$

where D is the diffusion rate constant.

Subsystem 5: auxin active transport mediated by PIN transporters

The rate of active transport from one cell to another is described by the following mass action equation:

$$V_{u,a} = K_{0,PIN} \cdot [a] \cdot [PIN] \quad (5)$$

where $[PIN]$ denotes concentration of the corresponding transporter (PIN1, PIN2, PIN3) and $K_{0,PIN}$ are the constants of active transport rate via the corresponding PIN ($K_{0,PIN1}$ for PIN1 and $K_{0,PIN3}$ for PIN3). As PIN2 mediates both shootward and inward auxin flows in epidermis, $V_{tr,a}$ is divided between the basipetal and lateral directions in the ratio

$$K_{0,bas,PIN2} : K_{0,lat,PIN2} = 7 : 3.$$

Subsystem 6: synthesis of PIN proteins

The synthesis rate of PIN proteins $V_{s,PIN}$ was approximated by the following Hill function taking into account the positive regulation by auxin:

$$V_{s,PIN} = K_{s,PIN} \frac{\left(\frac{[a]}{q_{1,PIN}}\right)^{s_{PIN}}}{1 + \left(\frac{[a]}{q_{2,PIN}}\right)^{s_{PIN}}} \quad (6)$$

where $K_{s,PIN}$ are the synthesis rate constants for the corresponding PINs (PIN1, PIN2, PIN3), $q_{1,PIN}$ are the thresholds of auxin-dependent activation of PIN synthesis, $q_{2,PIN}$ are the thresholds for saturation of auxin-dependent PIN1 synthesis and s_{PIN} are the Hill coefficients.

Subsystem 7: degradation of PINs

The rate of degradation for PIN proteins $V_{d,PIN}$ is defined by the rate equation:

$$V_{d,PIN} = K_{d,PIN} \cdot [PIN] \cdot f([a]), \quad (7)$$

where $K_{d,PIN}$ are the degradation constants of the corresponding PIN proteins (PIN1, PIN2, PIN3). As auxin regulates PIN1 and PIN2 degradation, the non-linear part of the degradation rate $f([a])$ was defined as:

$$f([a]) = 1 + \delta_{PIN}\left(\frac{[a]}{q_{3,PIN}}\right)^{h_{PIN}} \quad (8)$$

where $q_{3,PIN}$ are the thresholds of auxin-dependent PIN degradation, and h_{PIN} are the coefficients that define non-linearity of auxin-regulated PIN inhibition. The δ_{PIN} coefficients define if the PIN degradation is regulated by auxin ($\delta_{PIN1} = \delta_{PIN2} = 1$, $\delta_{PIN3} = 0$).

Model construction

Elementary subsystems 1–7 were used as the blocks for the 2-D dual-mechanism model construction according to the model configuration (Fig. 1). The rectangular cell layout consists of M layers ($j = 1, \ldots, M$) of N cells each ($i = 1 \ldots N$), where rows $j = 3, \ldots, M-2$ correspond to the central cylinder cells and rows $j = 1,\ 2,\ M-1,\ M$ correspond to epidermal tissues. Cells in layer $i = N$ are the most proximal cells of the root meristem, whereas cells in layer $i = 1$ are the root end. For all cells in the layout subsystems 2 and 3 are considered (in the basal variant of the model there is no auxin synthesis, eqn 2a). Also in all cells subsystems 4 and 5 operate taking into account the neighbours to which auxin moves by means of diffusion and active transport. In a cell of the central cylinder, subsystems 5–7 are integrated for PIN1 and PIN3, but for an epidermal cell subsystems 5–7 are defined for PIN2 and PIN3. Subsystem 1 is defined only for the $i = N$ cells of the central cylinder. The system of ordinary differential equations for the 2-D dual-mechanism model is assembled by summation of all rates (1–7) over the cellular layout (see Supplementary Data for details).

Parameter estimation

We used the experimental data of Vieten *et al.* (2005) as a basis for parameter estimation. The effective auxin concentrations for PIN upregulation revealed in the experiment are presented in Supplementary Data Table S1. We estimated the parameters for Hill functions so that the maxima of PIN expression *in silico* coincide with the effective auxin concentrations measured by Vieten *et al.* (2005). The other parameters were adjusted so that the patterns of PIN expression and auxin distribution qualitatively match the experimental data (Supplementary Data Table S2).

Numerical simulations

The non-linear system of equations of the model was integrated using the MGSModeller software package

(Likhoshvai *et al.*, 2001) on high-performance supercomputer cluster SSCC (Siberian Supercomputer Center). The dual-mechanism model calculation and analysis were repeated in the Matlab system (see Supplementary Data). Depending on the model configuration and the set of parameters, the calculations were done until a stationary solution was achieved (on average approx. 10^4 iterations).

The model simulation results were visualized using the Paraview program (Cedilnik *et al.*, 2006).

RESULTS

Cooperation of the reverse fountain and reflected flow mechanisms in the RAM

To investigate cooperation of the reverse fountain (Grieneisen *et al.*, 2007) and the reflected flow (Mironova *et al.*, 2010) mechanisms in the root meristem the 2-D dual-mechanism model was created as follows (see also Material and methods, Fig. 1). The dual-mechanism model is based on the 2-D reflected flow model structure (Mironova *et al.*, 2010), to which the processes of PIN2 and PIN3 expression were added to provide for shootward and lateral (outward/inward) auxin flows in the root meristem. The dual-mechanism model differs from the reverse fountain model in considering the dependence of PIN (PIN1, PIN2 and PIN3) expression on auxin concentration in a cell. Semi-quantitative estimation of the dependences were made by using the data from Vieten *et al.*, (2005) (Supplementary Data Table S1), who showed that the amounts of PIN transcripts and PIN proteins in the root meristem are strongly correlated with the concentration of exogenous auxin.

We adjusted the parameter values for the dual-mechanism model such that patterns of PIN expression and their mode of auxin dose dependence fit the experimental data (Fig. 1C, D; Supplementary Data). The dual-mechanism model with this set of parameters and initial uniform distribution of auxin and PIN protein concentrations in the cell layout yields a stationary solution with auxin and PIN protein patterns matching the experimentally observed ones (Fig. 2; Supplementary Data Video S1).

The values and the dimensionality of the effective auxin concentrations for upregulation of PINs revealed by Vieten *et al.* (2005) were used to estimate the values of variables in the dual-mechanism model. Auxin concentration was estimated as 0·4–1 μM in a vascular cell, 10–11 μM in the QC and 8–10 μM in a columella cell; PIN1 in a vascular cell was estimated as 2 μM, PIN2 in a epidermal cell as 0·4–1·2 μM and PIN3 in a columella cell as 0·4–0·65 μM. Note that the estimations may vary significantly by taking into account other processes that affect auxin transport. For example, the model does not reproduce high PIN3 expression in the central cylinder (Fig. 2C), where PIN3 may be upregulated by other mechanisms. It has been shown that cytokinin–auxin crosstalk antagonizes BRX

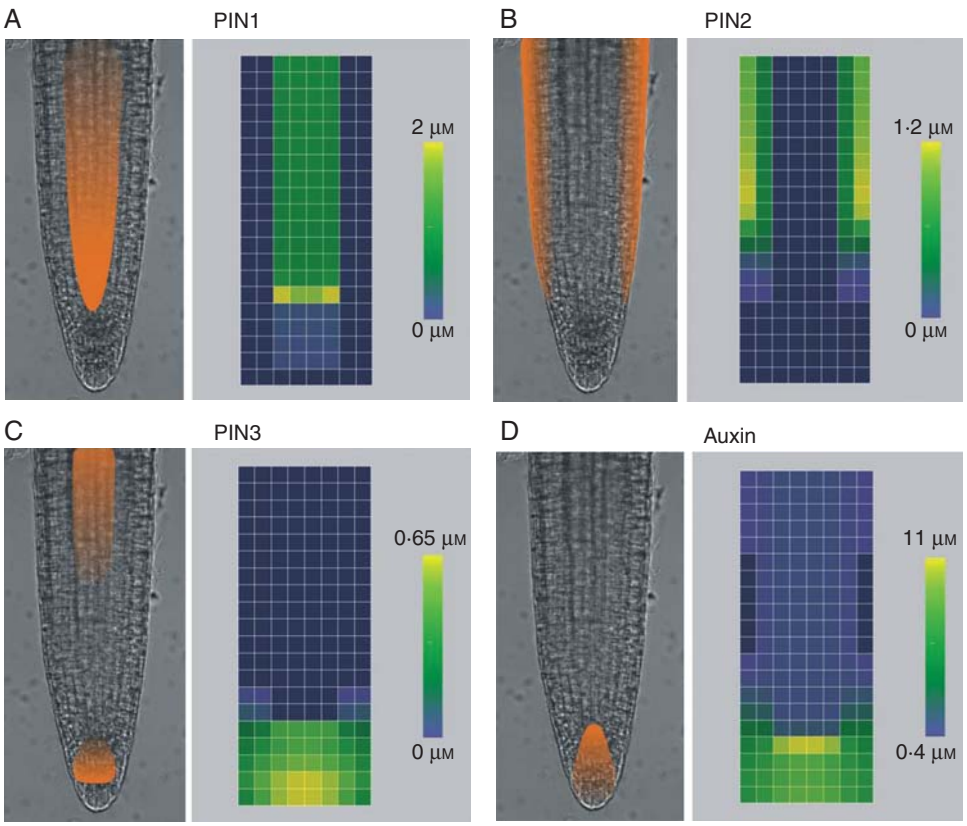

FIG. 2. The 2-D dual-mechanism model stationary solution. For each variable, a schematic representation of the expression pattern is given compared with the steady-state model solution. (A) PIN1 expression; (B) PIN2 expression; (C) PIN3 expression; (D) DR5 expression revealed *in vivo* and auxin distribution calculated *in silico*.

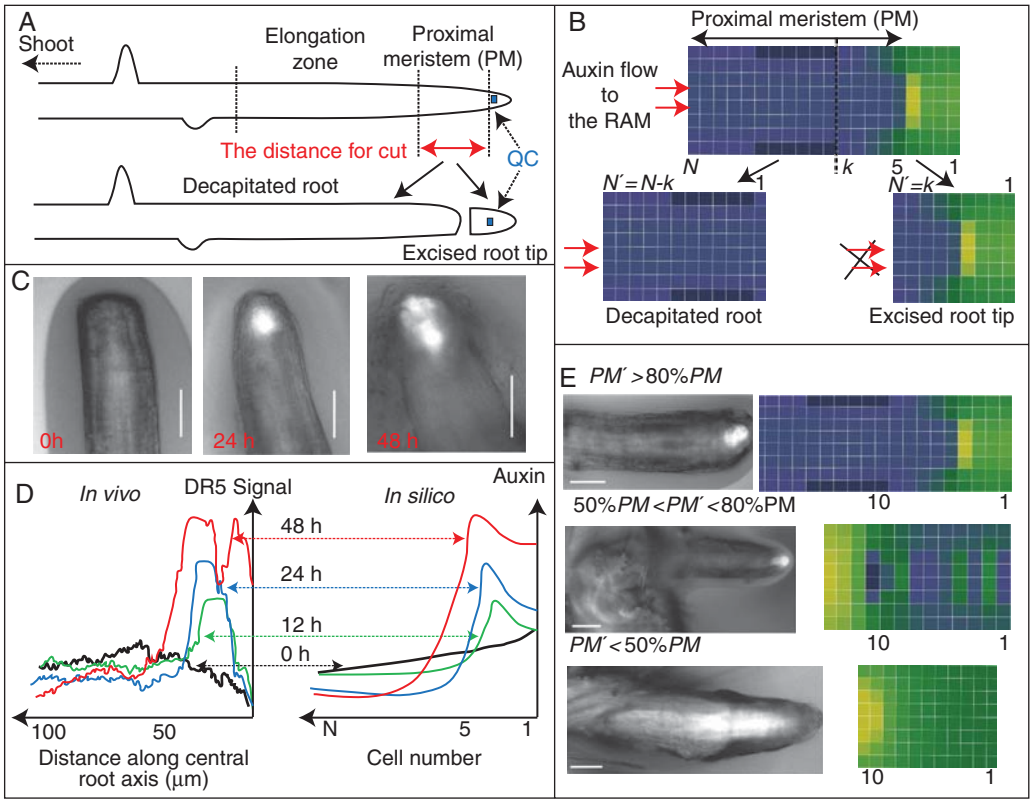

FIG. 3. *In vivo* and *in silico* experiment on RAM regeneration after root cutting. (A) Scheme of the *in vivo* experiment on root cutting. (B) Simulation scheme of root cut in the model. (C) Regeneration of the auxin response maximum in the decapitated root. (D) Correspondence between the *in vivo* and *in silico* results on changes in auxin response measured along the central root axis during regeneration of the decapitated root. Auxin (response) distribution is shown 2 d after cutting. Left: the dynamics of the DR5 signal along the central root axis of the regenerating RAM. Right: auxin distribution in the central cylinder layer $j = 4$ obtained at different time points of the model solution as the dual-mechanism model approached the stationary state. (E) Scheme of the model results on simulation of root regeneration after decapitation. Three different scenarios of the new root tip development were described dependent on the size of the PM that was left in the decapitated root both *in vivo* and *in silico*. Scale bar = 100 μm.

activity in the stele, which may affect PIN3 expression there (Scacchi *et al.*, 2010).

The mechanism of auxin distribution self-organization found in the resulting stationary solutions is as follows. At the first early phase, an auxin maximum is generated in the central cylinder cell array at a distance from the root end under the reflected flow mechanism (Mironova *et al.*, 2010). As a result, a zone of high auxin in the root tip is organized, which determines the peak of PIN3 synthesis. At the second phase, PIN3-mediated auxin redistribution is switched on in the root tip and auxin moves laterally from rootward flow and enters the epidermis where it is further involved in PIN2-based shootward flow. As PIN2 is localized also on the lateral internal cell sides in the epidermis, it redistributes auxin back to the rootward flow, finally completing the structure of the reverse fountain at the third phase.

Thus, our simulations demonstrate that the reflected flow and the reverse fountain may naturally cooperate in providing for establishment and further maintaining of the auxin pattern in the root tip.

Auxin redistribution after root cut

To estimate the advantage given by the cooperation of the two mechanisms, we made *in vivo* and *in silico* experiments on root cut. Root tip isolation abolishes the reflected flow mechanism in this tip, whereas cutting off the root tip damages the reverse fountain structure in the decapitated root.

In vivo *experiments on root cuttings.* We cut roots of DR5::GFP seedlings (3 dag) in such a way that both cuttings have part of the proximal meristem (PM) (Fig. 3A). Over the next 4 d we monitored reporter activity in both the decapitated root and the excised root tip.

In the tip of the decapitated root we observed a restoration of the auxin response peak followed by meristem regeneration. If the decapitated root contained less than half of the initial PM, the new root end shows high DR5 activity over the first 2 d, but the RAM never regenerates from it. If it contains between one-half and approx. four-fifths of the initial PM, the cut edge forms callus-like outgrowth first, followed by regeneration of the root meristem from the outgrowth periphery. The outgrowth cells have moderate and non-uniform DR5 activity, this activity increases in the regenerating meristem. Finally, if the new root end contains more than four-fifths of the PM, but still does not include the QC, root meristem regeneration occurs after 3 d without the callus stage. In this case, the dynamics of DR5 activity were similar to those observed by Xu *et al.* (2006) after QC laser ablation. During the first 12 h DR5 activity increased at the cut edge (Fig. 3C). The

region of DR5 activity expands in time so that the new auxin response peak was formed proximally to the cut edge in first 24 h. Auxin response maximum positioning and subsequent RAM regeneration occur over the next 48 h.

In the excised root tip the auxin pattern was maintained and the RAM remained viable for a long period of time. Although DR5 activity decreased over time (Fig. 4A–E), the signal was observed in the root tips at least for 4 d after cutting. The auxin response persists even in the shortest isolated tips without any vasculature.

In silico *experiments on RAM regeneration.* We simulated the auxin maximum restoration processes after root tip cut in the following manner (Fig. 3B). We first calculated the stationary auxin concentration $[a]_{i,j}$ in the dual-mechanism model at $M = 8$ and $N = 35$ and the set of parameters (Supplementary Data Table S2). The auxin distribution in the solution has a maximum in the 4th cells of the central cylinder (Fig. 2D). We than simulated the cut off root tip with a length of k cells and modelled the cell layout at $N' = 35 - k$. The calculations were made with the same set of parameters (Supplementary Data Table S2) but the initial data were $[a']_{i,j} = [a]_{i+k,j}$ and $[PIN']_{i,j} = [PIN]_{i+k,j}$, where $i = 1 \ldots 35 - k$ and the variable $[PIN]$ was $[PIN1]$, $[PIN2]$ or $[PIN3]$. The configuration of the model with the specified auxin and PIN distribution simulates the decapitated root tip. Note that in the initial model the length of the PM was $N-4 = 31$, where 4 cells is the length of the columella and QC. By cutting off the root tip of k cells in length, PM length in the decapitated root (PM') is $N - k$ cells.

Variation in k results in different auxin and PIN expression dynamics (Fig. 3E). If k was less than 12 cells ($PM' > 80\,\%$, which means that the decapitated root retained about 80 % of the intact PM) the stationary solution had an auxin maximum at a certain distance from the root end. The stable auxin maximum formed under the reflected flow mechanism as described in Mironova *et al.* (2010). In particular, the changes in auxin concentrations calculated in the model fit well to changes in DR5 activity detected *in vivo* during RAM regeneration (Fig. 3D). If k was varied between 12 cells and 20 cells ($50\,\% < PM' < 80\,\%$) damped oscillations of intracellular auxin concentrations with several auxin maxima appeared in the model solution with a high-amplitude zone in the middle of the proximal meristem (Supplementary Data Video 2). Finally, if k was greater than 20 cells ($PM' < 50\,\%$; more than half of the intact PM was removed), a stationary auxin distribution with the maximum in the most shootward cell of the PM (N') was formed, decreasing gradually toward the cut edge. These numerical results agree well with the experimental data (Fig. 3E) and thus explain most of the traits in the RAM regeneration processes (see Discussion).

In silico *experiments on excised root tips.* To simulate auxin distribution in the excised root tip we switched off the shoot-derived acropetal auxin flow in the model. In this case, the

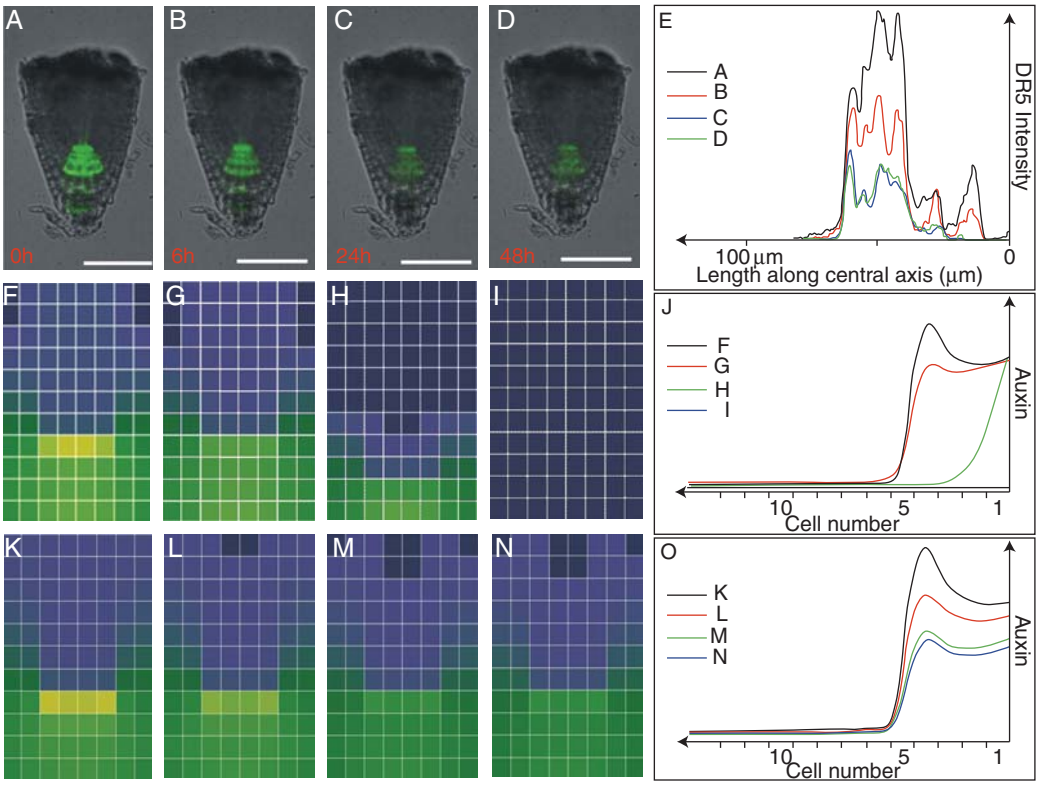

FIG. 4. *In vivo* and *in silico* experiments on the root tip excision. (A–D) Time series of the DR5::GFP-expressing excised root tip. (E) Dynamics of DR5 level along the central axis of the individual excised root from A–D. (F–I) Model solutions without biosynthesis obtained at different time points as the model approached the stationary state. (J) Auxin distribution in the central cylinder layer $j = 4$ of the solutions (F–I). (K–N) Simulation results of the model with auxin biosynthesis fitted to the experimentally observed data (A–D). (O) Auxin distribution in layer $j = 4$ of the model with auxin biosynthesis.

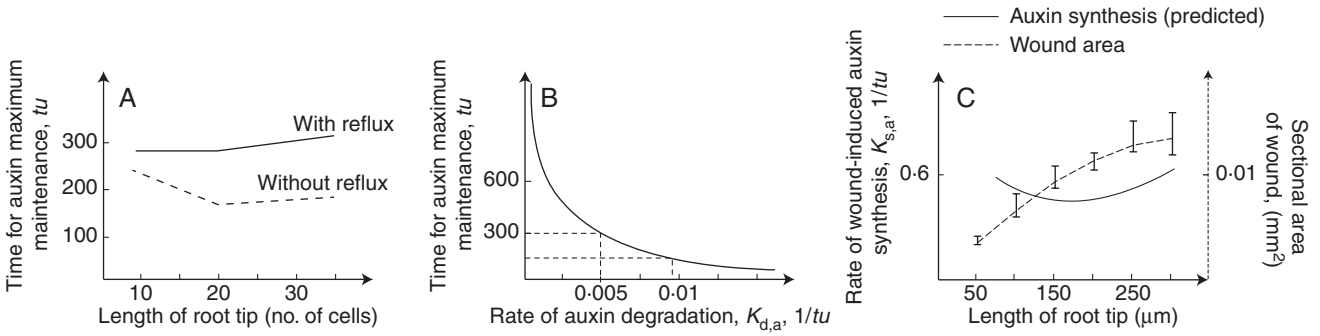

FIG. 5. *In silico* analysis of maintenance of the auxin maximum in the excised root tips under different conditions. (A) Time of maintenance of the auxin maximum in the model with or without reflux. (B) Stability of the auxin maximum under different rates of auxin degradation. (C) Estimated rates of wound-induced auxin synthesis for excised root tips of different lengths. Solid line: model prediction. Dashed black line: sectional area of the wound, $n = 10$. It is believed that the actual rates of wound-induced auxin synthesis must correlate positively with the area of the wound.

model calculation was started from the stationary solution with the auxin maximum in the fourth cells (Fig. 2D) with $\alpha = 0$ (other parameters remained unchanged; see Supplementary Data Table S2). We also simulated auxin distribution in the excised tips of different lengths. A set of models was created with cellular layouts that consist of a similar number of rows $M = 8$, but a different number of cells in a row $N = 10$, 20 and 35 (Supplementary Data Table S3). In the model solutions we observed a gradual decrease of auxin concentration in the root end (Fig. 4F–J), consistent with the experimentally observed decrease in DR5 activity over the first 2 d (Fig. 4A–C). However, *in silico* these dynamics were followed by the disappearance of the auxin maximum (Fig. 4I–J; Supplementary Data Video S3). This disappearance was only rarely observed *in vivo* during the first 5 d after excision (see following subsection). Despite this disagreement with the experimental data, due to the reflux in the epidermis the dual-mechanism model kept the auxin maximum in the excised root tip for a longer time as compared with the model without reflux (Fig. 5A), as was demonstrated by varying the constant for shootward active transport rate ($K_{0,\mathrm{lat,PIN2}}$) (Supplementary Data Table S3).

The role of auxin biosynthesis in maintenance of the auxin distribution pattern in the root

In the QC of the excised tips, DR5 activity was maintained for a long period (even increasing in the isolated radicles) despite the absence of a shoot-derived auxin supply. An intriguing example of the persistent auxin response was observed in the shortest excised tips, which consist only of promeristem and the root cap (Supplementary Data Fig. S1). Here DR5 activity in the tip is maintained for a long time despite the absence of both the reverse fountain and the reflected flow mechanism. Hydrolysis of auxin conjugates or auxin synthesis (wounding-induced or ubiquitous) in the excised root tips may cause the prolonged maintenance of the auxin maximum. We thus formed three hypotheses for the mechanisms that may prolong maintenance of the auxin maximum, tested them *in silico* and chose the most preferable.

Auxin conjugation is one of the pathways for auxin inactivation (reviewed by Ljung *et al.*, 2002; Woodward and Bartel, 2005). By decreasing the value for the auxin degradation rate $K_{d,a}$ we can simulate hydrolysis of auxin conjugates in the excised root tip. The decrease in $K_{d,a}$ prolonged maintenance of the auxin maximum in the tip (Fig. 5B). However, auxin conjugates are the finite resource, which will eventually run out without auxin biosynthesis. Thus, we conclude that hydrolysis of auxin conjugate may explain the short-lived maintenance of auxin distribution but cannot explain the prolonged DR5 activity in the excised root tip.

Auxin synthesis can be rapidly induced by wounding, directly at wounded sites (Sztein *et al.*, 2002; LeClere *et al.*, 2010). To test whether wounding-induced auxin synthesis is able to maintain the auxin maximum in the excised root tips, a number of modified models were created wherein auxin synthesis (eqn 2b) occurred in the last (*N*th) cells of the root tip for $N = 10$, 20 and 35 (see Supplementary Data). The rates of wound-induced auxin synthesis ($K_{s,a}$) cannot be measured directly so we estimated them from the stationary model solutions. The rates were estimated for excised roots of different lengths, by requiring that in each case the auxin maximum is maintained in stationary solutions despite the absence of shoot-derived auxin flow (Fig. 5C, solid curve). We can assume that the rates of wound-induced synthesis correlate with the cut sectional area, which in turn increases with the distance from the root end (Fig. 5C, dashed curve). However, the length of the excised root tips did not correlate with the rates of wound-induced auxin synthesis estimated in the model and estimated on the basis of the cut sectional area (Fig 5C; Supplementary Data Table S3). Thus, although wound-induced auxin synthesis has an impact on auxin supply in the excised tip, this effect is not sufficient to produce the experimentally observed data.

Cells of all types in the root tip have the capacity for auxin synthesis and this capacity contributes substantially to robust auxin gradients in the root tip (Ljung *et al.*, 2005; Petersson *et al.*, 2009). To test the role of the ubiquitous auxin synthesis *in silico* we created a modified model in which all cells ubiquitously produce auxin at a low rate (eqn 2b). The model parameters for auxin synthesis and shoot-derived auxin flow to the RAM were adjusted in this model to obtain the auxin maximum in the fourth cells of the central cylinder (Supplementary Data Table S3). Simulation of the root tip cut was then performed as described in the previous section for $N = 10$, 20 and 35 cells. Unlike the case of wound-induced

synthesis, in this case, the rates of auxin synthesis were the same for root tips of different lengths (Supplementary Data Table S3). In the model solutions we observed an overall decrease in auxin content at the root end, although the concentration maximum was still located in the 4th cells (Fig. 4K–O; Supplementary Data Video S4). Moreover, the model with ubiquitous auxin synthesis equilibrates faster while simulating auxin distribution in intact and decapitated root, a possible adaptive feature of the system (data not shown).

Our simulations demonstrate that compared with hydrolysis of auxin conjugates and wound-induced synthesis, ubiquitous auxin biosynthesis is the preferable mechanism for maintenance of the auxin maximum in the excised root tips. Thus, auxin biosynthesis appeared to be a third force of equal importance to the reverse fountain and reflected flow mechanisms for auxin patterning in the RAM.

DISCUSSION

Experiments on cut roots to study meristem regeneration and maintenance are classical in plant developmental biology (Torrey, 1957; Feldman, 1980; Ivanov, 2007). The molecular mechanisms governing RAM development and maintenance are orchestrated by the hormone auxin (Sabatini *et al.*, 1999; Blilou *et al.*, 2005; Tanaka *et al.*, 2006; Peer *et al.*, 2011). Auxin can be regarded as a morphogen, which is involved in establishment of patterns of cell identities within developing plant organs (Benkova *et al.*, 2009; Wolpert, 2011). A unique feature of auxin is its tightly regulated cell-to-cell polar transport, which allows auxin to generate gradients and maxima in a particular tissue and contribute to tissue patterning in a dose-dependent manner (Peer *et al.*, 2011). Redistribution of the auxin gradient provides positional information for root regeneration (Xu *et al.*, 2006; Sena *et al.*, 2009; Mironova *et al.*, 2010). Auxin regulates expression of its own transporters. At relatively low level, auxin upregulates PIN family transporters (Vieten *et al.*, 2005). Polar localization of PIN proteins on the cell membrane may also be upregulated by auxin (Paciorek *et al.*, 2005; Sauer *et al.*, 2006). A negative effect of high auxin doses to PIN expression and polarization has also been shown by Vieten *et al.* (2005).

An understanding of the complex interplay of auxin transportation mechanisms requires the application of sophisticated methods. Auxin distribution has been simulated in mathematical models predicting significant mechanisms for phyllotaxis (Jönsson *et al.*, 2006; Sahlin *et al.*, 2009), tissue polarization (Wabnik *et al.*, 2010), leaf venation (Feugier *et al.*, 2006; Bayer *et al.*, 2009), shoot branching (Prusinkiewicz *et al.*, 2009) and root development (Swarup *et al.*, 2005; Grieneisen *et al.*, 2007; Laskowski *et al.*, 2008; Mironova *et al.*, 2010; Band and King, 2012). Two conceptual models have been proposed to explain the mechanism of auxin maximum formation in the RAM: the reverse fountain and the reflected flow. The reverse fountain (Grieneisen *et al.*, 2007) is a structural mechanism which implies that the RAM structure determines the auxin distribution pattern. The reflected flow (Mironova *et al.*, 2010) is a morphogenetic mechanism which establishes positional information for RAM patterning. It seems intuitively likely that both structural and morphogenetic mechanisms act in the root, providing for self-organization and subsequent self-maintenance of the RAM. Here we combine the two mechanisms in one model to test whether they cooperate and what processes in RAM development they jointly explain.

The mechanisms of the reverse fountain and reflected flow naturally cooperate in intact roots

For the dual-mechanism model we used the same cellular layout as in the reflected flow model (Fig. 1A; Mironova *et al.*, 2010). Only two cell types were considered: central cylinder cells and epidermal cells. PIN1 was the auxin transporter in the reflected flow model. In the dual-mechanism model two additional auxin transporters, PIN2 and PIN3, were included to mediate shootward and lateral (outward/inward) auxin transport. The dual-mechanism model integrates up-to-date experimental data on auxin-regulated PIN1–PIN3 expression (Fig. 1B–D). The model parameters for PIN expression were estimated so that the effective auxin concentrations for PIN regulation calculated *in silico* match those reported *in vivo* by Vieten *et al.* (2005; see Supplementary Data). In the model solution we observed formation of PIN1, PIN2 and PIN3 expression domains together with auxin distribution pattern, both agreeing well with the experimental data (Fig. 2).

We suggest that the two mechanisms may naturally cooperate *in vivo* due to auxin-regulated expression of its own transporters. By using model analysis we estimated the concentration of auxin, PIN1, PIN2 and PIN3 in different RAM tissues. The estimated auxin concentrations (0·4–1 μM in a vascular cell; 10–11 μM in the QC and 8–10 μM in a columella cell) agree well with the following constraints from independent data. DR5 reporter expression pattern was demonstrated to reflect free-auxin concentrations between 10^{-8} and 10^{-4} M (Ulmasov *et al.*, 1997; Sabatini *et al.*, 1999). Also, Petersson *et al.* (2009) showed that the concentration of intracellular indole-3-acetic acid in the RAM is in the range 1–50 μM.

In numerical experiments simulating self-organization of auxin distribution in an initially unspecialized tissue, we observed generation of an auxin distribution pattern that matches the experimentally known expression of DR5. The auxin maximum peak in the root tip is formed under the reflected flow mechanism, which may operate from the earliest stages of root development. Thus, cells of the developing root can acquire positional information sufficient for RAM patterning. Moreover, in the model solution all necessary features for the functioning of the reverse fountain were organized by the reflected flow mechanism. So, the further maintenance of the auxin maximum at later developmental stages can be provided mainly by the reverse fountain structural mechanism. The auxin gradient in the PM is also organized by the reverse fountain. However, the reflected flow mechanism does not disappear even after formation of the RAM structure. The morphogenetic mechanism continues to function, revealing itself if the RAM structure is disrupted or the environment changes. For example, the mechanism is crucial for RAM re-specification after NPA (naphthylphthalamic acid) treatment (Mironova *et al.*, 2010) or regeneration of the RAM in decapitated root.

The next step for model testing was a validation experiment to test whether the model would fit the evidence and provide reliable predictions. For the dual-mechanism model, experiments on root cut are germane. Performed from the beginning of the 19th century in many labs, experiments on the regeneration of the decapitated root and on the viability of the excised root tips outlined phenomenologically the steps occurring in the two root fragments. The advance in this class of experiment here was in using DR5::GFP *A. thaliana* plants that reveal an auxin response gradient in addition to classical phenomenology.

The mechanism for auxin distribution self-organization in the proximal meristem of decapitated roots

Previously, two main types of root restoration in decapitated roots were reported. If the removed part is sufficiently large (proximal cuts, for example 1 mm for *Vicia faba* or 700–750 μm for *Zea mays*) then lateral roots formed close to the cut edge (Feldman, 1980). However, removal of a smaller length of root tip (distal cuts, for example 450 μm for *Z. mays*) led to regeneration of the root tip, aligned with the main axis of the root. Distal cuts were carefully investigated by Sena *et al.* (2009) and it was shown that the region of high regeneration competence in the *A. thaliana* root was located in the distal PM (up to 130 μm from the root end), the frequency of regeneration decreased by a factor of ten more proximally (at 200 μm from the root end) and dropped to zero at 270 μm. Feldman (1980) showed that in distal cuts the part of the PM left in the decapitated root should exceed some critical size for root tip regeneration to occur. It was also shown that regeneration of the apex arises from the actively proliferating PM cells.

In our *in silico* and *in vivo* experiments we found three types of response (Fig. 3E). No regeneration occurred *in vivo* if the decapitated root had less than half of the initial PM. Decapitated roots containing approx. 50–80 % of the PM first formed a callus-like outgrowth from which a new root tip appeared. The meristems of decapitated roots containing more than 80 % of the PM regenerated similarly to observations for QC laser ablation (Xu *et al.*, 2006).

Based on our numerical experiments we propose a mechanism explaining the existence of these three different scenarios of new root tip development and their dependence on the size of the PM that was left in the decapitated root. The key role is played by shoot-derived auxin flow to the RAM, which was not changed by decapitation. If the major part (more than half) of the PM was lost, auxin flow from the elongation zone was too high to be assimilated in the remaining part of the PM so that the cells of PM accumulated auxin and this did not facilitate meristem restoration. In contrast, if the major part of the PM was left in the decapitated root, the auxin transport system (namely, the reflected flow mechanisms) was able to cope with the rootward auxin flow, generating an auxin maximum at a distance from the root edge. In intermediate cases, we observed *in silico* damped auxin oscillations with several unstable maxima caused by disturbance of the auxin traffic. We suggest that the damped oscillations predetermine callus-like outgrowth. In fact, discordant positional information due to temporally varying auxin maxima may cause outgrowth cell specialization, making these cells different in size and DR5 level.

Excised root tip as an autonomous organ

Prolonged maintenance of RAM viability in excised root tips has been known for almost a century (reviewed by Torrey, 1957). Study of the role of auxin in RAM stem cell niche maintenance has become possible in recent years using auxin sensors. Grieneisen *et al.* (2007) showed maintenance of the auxin maximum in dissected roots from shoots.

Here we describe for the first time the dynamics of DR5 activity in excised root tips of different lengths. Taking into account that DR5 is a promeristem marker, the experimental results provide evidence for prolonged maintenance of the stem cell niche in the excised root tips. The auxin response maximum is maintained even in the shortest tips lacking any PM.

Grieneisen *et al.* (2007) suggested that the reverse fountain mechanism provides for a stable auxin maximum in dissected roots. Consequently, we tested whether this feature is applicable to the dual-mechanism model. The model showed that the reverse fountain mechanism has a significant impact on auxin gradient maintenance in the excised root, which depends on the length of the root tip (Fig. 5A). However, in numerical simulation the gradual drop in auxin concentration causes the eventual disappearance of the auxin maximum. This simulation result suggests that the reverse fountain and the reflected flow together were not enough to describe the whole set of experimental data. Here we explored *in silico* three possible hypotheses for maintenance of the auxin maximum in excised root tips: (1) auxin conjugates hydrolysed back to the free hormone can act as sources of free auxin; (2) wounding-induced auxin synthesis supports the maximum; and (3) the existence of a basal auxin synthesis in root cells.

Our simulations showed that three mechanisms have different impacts on the maintenance of the spatial distribution of auxin. As auxin conjugates are a finite resource, their hydrolysis can account only for the maintenance of the auxin pattern for a short period. Soeno *et al.* (2010) demonstrated that after treatment of seedlings with an inhibitor of auxin biosynthesis, endogenous auxin levels in roots decreased to less than 10 % of the levels in the controls, indicating that auxin synthesized *de novo* is the main auxin source for roots.

The root tip has the ability to synthesize auxin (van Overbeek, 1939; Feldman, 1980; Ljung *et al.*, 2005; Stepanova *et al.*, 2008; Petersson *et al.*, 2009). van Overbeek (1939) proposed that the excised root tip is maintained alive due to continuing auxin biosynthesis. The question is whether it is a wound-induced synthesis or is there a basal capacity for auxin synthesis in root cells. Our numerical experiments confirm that wound-induced auxin synthesis is not the main contribution for auxin supply to the excised root tip. For this to occur, the rates of auxin synthesis at the wounded sites would have to be higher for small wounds and lower for large wounds.

Auxin synthesis was found in both meristematic and non-meristematic parts of the root, indicating that there is basal auxin synthesis in root cells (Ljung *et al.*, 2005). Our simulations showed that this basal auxin synthesis together with the

reverse fountain allows the auxin gradient to form, with a maximum at the 4th–5th cell from the root end in the excised root tips. The more PM was left in the excised root tip, the more impact the reverse fountain has in maintaining the auxin gradient. Basal auxin synthesis can explain maintenance of the auxin maximum in very short excised roots, which contain only QC and the root cap (neither the reflected flow nor the reverse fountain mechanism work in excised root tips of this type). In our simulations we showed that the auxin distribution equilibrates faster if we take into account auxin biosynthesis. This can be an adaptive feature for RAM development. Rowntree and Morris (1979) showed that ^{14}C applied to apical pea buds accumulated in the lateral root primordia but not in the root tip of the primary root nor, in older plants, in the tips of the lateral roots. These data support the idea that the root tips are autonomous from shoot-derived rootward auxin flow because of *de novo* auxin synthesis therein. This explains why the auxin gradient persists in the root tip of the excised root.

Several recent studies have revealed auxin biosynthesis mechanisms in root (Ljung *et al.*, 2005; Stepanova *et al.*, 2008). Here we suggest that auxin biosynthesis is a third main force in auxin gradient formation along with the reflected flow and reverse fountain transportation mechanisms. We showed that the mechanisms cooperate, providing for a semi-autonomous RAM with the ability to self-regenerate.

SUPPLEMENTARY DATA

Supplementary data are available online at www.aob.oxfordjournals.org and include: a description of the 2-D dual mechanism model; the dual-mechanism model reduction to the reverse fountain model; parameter estimation (incorporating Table S1: parameter estimation for the dual-mechanism model, and Table S2: the basic set of model parameters for the 8×20 2-D dual-mechanism model); simulation of auxin distribution in the excised root tips (incorporating Table S3: parameter values for the model's modifications); and Fig. S1: auxin response maintenance in the shortest excised root tips. Video S1: simulation of auxin patterning in the dual-mechanism model. PIN1, PIN2 and PIN3 expression domains and the pattern of auxin distribution are self-organized in the *in silico* root. Video S2: oscillations in auxin concentration simulated in the decapitated root may predetermine callus-like outgrowth. The model was run from the reduced cellular layout with the same intensity of auxin influx to the RAM. Video S3: changes in auxin distribution in model simulation without auxin biosynthesis. Simulation in the root tips of different lengths is presented. Video S4: comparison of the maintenance of the auxin maximum in excised root tips with and without auxin biosynthesis.

ACKNOWLEDGMENTS

We thank S. I. Baiborodin, S. S. Ibragimova, A. Ermakov and S. S. Sangaev for technical support and the anonymous reviewers for valuable advice. Microscopy was performed in the Shared Facility Center for Microscopic Analysis of Biological Objects SB RAS. Numerical calculations were performed on the supercomputer cluster of the Shared Facility Center for Bioinformatics SB RAS. This study was supported by RFBR grants 11-04-01254a and 10-01-00717, Dynasty Foundation grant for young biologists, Russian Ministry of Education No. 07·514·11·4023, 07·514·11·4052, P857, Integration projects SB RAS 80, The Russian President grant SS-5278·2012·4 and RAS program A.II.6, 'Molecular and Cellular Biology'. E.M. was supported by NIH grant R01GM086883.

LITERATURE CITED

Band LR, King JR. 2011. Multiscale modelling of auxin transport in the plant-root elongation zone. *Journal of Mathematical Biology*, doi:10.1007/s00285-011-0472-y. http://www.springerlink.com/content/x74n1467354q6075/.

Baskin T, Peret B, Baluška F, *et al*. 2010. Shootward and rootward: peak terminology for plant polarity. *Trends in Plant Science* **15**: 593–594.

Bayer EM, Smith RS, Mandel T, *et al*. 2009. Integration of transport-based models for phyllotaxis and midvein formation. *Genes and Development* **23**: 373–384.

Benkova E, Michniewicz M, Sauer M, *et al*. 2003. Local, efflux-dependent auxin gradients as a common module for plant organ formation. *Cell* **115**: 591–602.

Benkova E, Ivanchenko MG, Friml J, Shishkova S, Dubrovsky JG. 2009. A morphogenetic trigger: is there an emerging concept in plant developmental biology? *Trends in Plant Science* **14**: 189–193.

Bennett MJ, Marchant A, Green HG, *et al*. 1996. Arabidopsis AUX1 gene: a permease-like regulator of root gravitropism. *Science* **273**: 948–950.

Blilou I, Xu J, Wildwater M, *et al*. 2005. The PIN auxin efflux facilitator network controls growth and patterning in Arabidopsis roots. *Nature* **433**: 39–44.

Brunoud G, Wells D, Oliva M, *et al*. 2012. A novel sensor to map auxin response and distribution at high spatio-temporal resolution. *Nature* **482**: 103–106.

Cedilnik A, Geveci B, Moreland K, Ahrens J, Favre J. 2006. Remote large data visualization in the ParaView framework. In: Heirich A, Raffin B, dos Santos LP. eds. *Eurographics Symposium on Parallel Graphics and Visualization*. Geneva: Eurographics, 162–170.

Dolan L, Janmaat K, Willemsen V, *et al*. 1993. Cellular organisation of the *Arabidopsis thaliana* root. *Development* **119**: 71–84.

Feldman LJ. 1980. Auxin biosynthesis and metabolism in isolated roots of *Zea mays*. *Physiologia Plantarum* **49**: 45–150.

Feugier FG, Iwasa Y. 2006. How canalization can make loops: a new model of reticulated leaf vascular pattern formation. *Journal of Theoretical Biology* **243**: 235–244.

Friml J, Benkova E, Blilou I, *et al*. 2002. AtPIN4 mediates sink-driven auxin gradients and root patterning in Arabidopsis. *Cell* **108**: 661–673.

Friml J, Vieten A, Sauer M, *et al*. 2003. Efflux-dependent auxin gradients establish the apical–basal axis of Arabidopsis. *Nature* **426**: 147–153.

Geisler M, Murphy AS. 2006. The ABC of auxin transport: the role of p-glycoproteins in plant development. *FEBS Letters* **580**: 1094–1102.

Grieneisen VA, Xu J, Marée AF, Hogeweg P, Scheres B. 2007. Auxin transport is sufficient to generate a maximum and gradient guiding root growth. *Nature* **449**: 1008–1013.

Ikeda Y, Men S, Fischer U, *et al*. 2009. Local auxin biosynthesis modulates gradient-directed planar polarity in Arabidopsis. *Nature Cell Biology* **11**: 731–738.

Ivanov VB. 2007. Oxidative stress and formation and maintenance of root stem cells. *Biochemistry (Moscow)* **72**: 1110–1114.

Jiang K, Feldman LJ. 2005. Regulation of root apical meristem development. *Annual Review of Cell Development Biology* **21**:485–509.

Jönsson H, Heisler MG, Shapiro BE, Meyerowitz EM, Mjolsness E. 2006. An auxin-driven polarized transport model for phyllotaxis. *Proceedings of the National Academy of Sciences USA* **103**: 1633–1638.

Kim JI, Murphy AS, Baek D, *et al*. 2011. YUCCA6 over-expression demonstrates auxin function in delaying leaf senescence in *Arabidopsis thaliana*. *Journal of Experimental Botany* **62**: 3981–3992.

Laskowski M, Grieneisen VA, Hofhuis H, *et al*. 2008. Root system architecture from coupling cell shape to auxin transport. *PLoS Biology* **6**: e307. http://dx.doi.org/10.1371/journal.pbio.0060307.

LeClere S, Schmelz E, Chourey P. 2010. Sugar levels regulate tryptophan-dependent auxin biosynthesis in developing maize kernels. *Plant Physiology* **153**: 306–318.

Likhoshvai VA, Matushkin YG, Ratushny AV, Ananko EA, Ignatieva EV, Podkolodnaya OA. 2001. Generalized chemokinetic method for gene network simulation. *Russian Journal of Molecular Biology* **35**: 919–926.

Likhoshvai VA, Omelianchuk NA, Mironova VV, Fadeev SI, Mjolsness ED, Kolchanov NA. 2007. Mathematical model of auxin distribution in the plant root. *Russian Journal of Developmental Biology* **38**: 446–456.

Ljung K, Hull AK, Kowalczyk M, *et al*. 2002. Biosynthesis, conjugation, catabolism and homeostasis of indole-3-acetic acid in *Arabidopsis thaliana*. *Plant Molecular Biology* **49**: 249–272.

Ljung K, Hull AK, Celenza J, *et al*. 2005. Sites and regulation of auxin biosynthesis in Arabidopsis roots. *The Plant Cell* **17**: 1090–1104.

Mironova VV, Omelyanchuk NA, Yosiphon G, *et al*. 2010. A plausible mechanism for auxin patterning along the developing root. *BMC Systems Biology* **4**: 98. http://dx.doi:10.1186/1752-0509-4-98.

van Overbeek J, 1939. Auxins. *The Botanical Review* **25**: 269–350.

Paciorek T, Zazímalová E, Ruthardt N, *et al*. 2005. Auxin inhibits endocytosis and promotes its own efflux from cells. *Nature* **435**: 1251–1256.

Peer WA, Blakeslee JJ, Yanga H, Murphy AS. 2011. Seven things we think we know about auxin transport. *Molecular Plant* **4**: 487–504.

Petersson S, Johansson A, Kowalczyk M, *et al*. 2009. An auxin gradient and maximum in the *Arabidopsis* root apex shown by high-resolution cell-specific analysis of IAA distribution and synthesis. *The Plant Cell* **21**: 1659–1668.

Petrásek J, Mravec J, Bouchard R, *et al*. 2006. PIN proteins perform a rate-limiting function in cellular auxin efflux. *Science* **312**: 914–918.

Prusinkiewicz P, Crawford S, Smith RS, *et al*. 2009. Control of bud activation by an auxin transport switch. *Proceedings of the National Academy of Sciences USA* **106**: 17431–17436.

Rowntree RA, Morris DA. 1979. Accumulation of ^{14}C from exogenous labeled auxin in lateral root primordial of intact pea seedlings (*Pisum sativum* L.). *Planta* **144**: 463–466.

Sabatini S, Beis D, Wolkenfelt H, *et al*. 1999. An auxin-dependent distal organizer of pattern and polarity in the *Arabidopsis* root. *Cell* **99**: 463–472.

Sahlin P, Söderberg B, Jönsson H. 2009. Regulated transport as a mechanism for pattern generation: capabilities for phyllotaxis and beyond. *Journal of Theoretical Biology* **258**: 60–70.

Sauer M, Balla J, Luschnig C, *et al*. 2006. Canalization of auxin flow by Aux/IAA-ARF-dependent feedback regulation of PIN polarity. *Genes & Development* **20**: 2902–2911.

Scacchi E, Salinas P, Gujas B,, *et al*. 2010. Spatio-temporal sequence of cross-regulatory events in root meristem growth. *Proceedings of the National Academy of Sciences USA* **107**: 22734–22739.

Sena G, Wang X, Liu H, Hofhuis H, Birnbaum KD. 2009. Organ regeneration does not require a functional stem cell niche in plants. *Nature* **457**: 1150–1153.

Soeno K, Goda H, Ishii T, *et al*. 2010. Auxin biosynthesis inhibitors, identified by a genomics-based approach, provide insights into auxin biosynthesis. *Plant Cell Physiology* **51**: 524–536.

Stepanova AN, Robertson-Hoyt J, Yun J, *et al*. 2008. TAA1-mediated auxin biosynthesis is essential for hormone crosstalk and plant development. *Cell* **133**: 177–191.

Swarup R, Bennett M. 2003. Auxin transport: the fountain of life in plants? *Developmental Cell* **5**: 824–826.

Swarup R, Kramer E, Perry P, *et al*. 2005. Root gravitropism requires lateral root cap and epidermal cells for transport and response to a mobile auxin signal. *Nature Cell Biology* **7**: 1057–1065.

Sztein AE, Ilic N, Cohen JD, Cooke TJ. 2002. Indole-3-acetic acid biosynthesis in isolated axes from germinating beans seeds: the effect of wounding on the biosynthetic pathway. *Plant Growth Regulation* **36**: 201–207.

Tanaka H, Dhonukshe P, Brewer P, Friml J. 2006. Spatiotemporal asymmetric auxin distribution: a means to coordinate plant development. *Cellular and Molecular Life Sciences* **63**: 2738–2754

Torrey JG. 1957. Auxin control of vascular pattern formation in regenerating pea root meristems grown *in vitro*. *American Journal of Botany* **44**: 859–870.

Ugartechea-Chirino Y, Swarup R, Swarup K. 2010. The AUX1 LAX family of auxin influx carriers is required for the establishment of embryonic root cell organization in *Arabidopsis thaliana*. *Annals of Botany* **105**: 277–289.

Ulmasov T, Murfett J, Hagen G, Guilfoyle T. 1997. Aux/IAA proteins repress expression of reporter genes containing natural and highly active synthetic auxin response elements. *The Plant Cell* **9**: 1963–1971.

Vieten A, Vanneste S, Wisniewska J, *et al*. 2005. Functional redundancy of PIN proteins is accompanied by auxin dependent cross-regulation of PIN expression. *Development* **132**: 4521–4531.

Wabnik K, Kleine-Vehn J, Balla J, *et al*. 2010. Emergence of tissue polarization from synergy of intracellular and extracellular auxin signaling. *Molecular Systems Biology* **6**: 447. http://dx.doi.org/10.1038/msb.2010.103.

Wisniewska J, Xu J, Seifertova D, *et al*. 2006. Polar PIN localization directs auxin flow in plants. *Science* **312**: 858–860.

Wolpert L. 2011. Positional information and patterning revisited. *Journal of Theoretical Biology* **269**: 359–365.

Woodward AW, Bartel B. 2005. Auxin: regulation, action, and interaction. *Annals of Botany* **95**: 707–735.

Xu J, Hofhuis H, Heidstra R, Sauer M, Friml J, Scheres B. 2006. A molecular framework for plant regeneration. *Science* **311**: 385–388.

Zažímalová E, Murphy A, Yang H, Hoyerová K, Hošek P, 2010. Auxin transporters—why so many? *Cold Spring Harbor Perspectives in Biology* **2**: a001552. http://dx.doi.or/10.1101/cshperspect.a001552.